Journal of Information Systems Engineering and Management
2025, 10(30s)
e-ISSN: 2468-4376
https://www.jisem-journal.com/

Research Article

Deep learning -Based Control and Management of grid connected hybrid renewable energy system

[1]Ramesh T, [2]Balachander K
[1] *Research Scholar, Department of EEE, Faculty of Engineering, Karpagam Academy of Higher Education Coimbatore, Tamilnadu, India*
Your.ramesh83@gmail.com
[2]*Department of EEE, Faculty of Engineering, Karpagam Academy of Higher EducationCoimbatore, Tamilnadu, India*
kaybe.ind@gmail.com

ARTICLE INFO

Received: 30 Dec 2024

Revised: 16 Feb 2025

Accepted: 25 Feb 2025

ABSTRACT

Hybrid renewable energy sources (HRESs), including wind and photovoltaic systems (PV), are gaining popularity as alternatives to traditional sources for power in distributed generation, with the integration of energy storage systems(BAT) enhancing their effectiveness, such as battery, are important for ensuring equilibrium between the variable nature of energy production and the changing conditions of dynamic RL load. The situation demands sophisticated power control and management strategies to address difficult circumstances. This study examines and assesses an effective method for regulating DC bus voltage and enhancing power quality under conditions of dynamic load variation. The proposed power management strategy for hybrid renewable energy systems uses a deep learning intelligent controller, particle swarm optimization (PSO), Recurrent Neural Networks (RNN) and Convolution Neural Networks (CNN), creating an innovative an oversight power management structure designed for photovoltaic systems equipped with battery storage. The goal is to maintain consistent power flow, ensure quality through Total Harmonic Distortion, and ensure uninterrupted service by preventing system components from exceeding operational limits, enhancing DC link bus voltage regulation in renewable hybrid systems.

Keywords: PV, Wind, Battery, dc/dc Converter, VSI, PI-PSO,RNN,and CNN.

I. INTRODUCTION

Global warming, the depletion of fossil fuel supplies, and rising energy use highlight the importance of renewable energy alternatives must be developed. Using data at several sites to guide operating choices, Author [1] created a hybrid wind-PV system for effective power management, showcasing an innovative method to power management. A BAT-Fuzzy control approach is put out by **[2]** for a HRESs that integrates a PV with BES. The best parameter values for MPPT are found using the fuzzy controller and the BAT method. Simulations demonstrate improved stability and quick reaction in transient situations. An experimental investigation on a freestanding hybrid micro grid system using RES as wind turbines, PV, fuel cells (FC), and BAT was carried out by [3]. The hybrid system, designed for distant applications, utilizes speed controllers for wind and SIFL controllers for solar subsystems, and An energy management approach that focuses on the charge level of batteries. **[4]** Explore optimal design, power management, and control strategies for hybrid Grid-tied PV and BAT storage of energy and wind power conversion systems. This research aims to maintain stable DC-link voltage, smooth stator and rotor currents, and steady active power output using a moth-flame optimized fuzzy logic controller. A hybrid system that combines biomass, PV, WT, and battery storage is suggested by **[5].** For the suggested hybrid setup, four optimization techniques are employed to maximize performance, guaranteeing that energy demands are satisfied while lowering COE. In this paper [6] improve CNN-LSTM hyper parameters using Coati optimization method in enhancing performance and learning rate in solar and wind power forecasting. An ANFIS controller and Management technique for supervisory power regulation are used in the work by [7] to investigate a method for controlling DC bus voltage in solar systems. By keeping system components from going above operating thresholds, the objective is to maintain steady power flow and guarantee

continuous service. The intelligent control of the SEPIC Converter in electric car charging systems is examined in a research by [8]. In order to solve imbalance issues and accomplish sustainable development objectives, they employ a proportional-integral controller and calculated state of charge. By merging CNN and DQN in a hybrid architecture, **[9]** created a power management method that outperformed conventional models with A processing duration of 0.2 seconds accompanied by an energy dissipation of 0.01 megawatts. In this manuscript **[10]** trained and validated models for forecasting future energy consumption using convolution neural networks utilizing data from Pennsylvania's "ensue" dataset and The 'International Renewable Energy Agency' evaluated the models' performance using criteria This encompasses metrics like mean absolute error, average squared error, root mean square error, and average constant error expressed as a percentage. Author [11] highlight power quality issues in photovoltaic micro grids due to changes in solar irradiance, load fluctuations, and switching activities. Deep learning, using MATLAB, enhances disturbance detection and classification using Hamiltonian Deep Neural Networks (HDNN). The study explores energy consumption, scheduling, and management in demand response systems for electric utilities, incorporating alternative energy sources like PV, thermal, CHP, and wind. It uses heuristic algorithms for smart appliance scheduling and management. The study by **[13]** proposes a strategy to enhance grid stability by integrating Energy Storage Systems with a Pyramidal Dilation Attention Convolutional Neural Network, thereby reducing electricity expenses. An ANFIS method is used in the work by [**14]**to predict the instantaneous photovoltaic power database and optimize the size of solar panel-battery systems and energy management in smart grids. The 2023 research by [15] addresses the issues with micro grid systems by emphasizing network designs, peak-shaving and optimum power flow. They point to block chain technology, metaheuristic techniques, and reinforcement learning as viable options for energy management, decentralization, and cybersecurity in microgrid systems. An overview of micro grids is given by **[16],** who concentrate on their energy management techniques and operating procedures. In order to ensure utility providers' profitability, the energy management system (EMS) plays a crucial role in balancing energy resources such as distributed generation, conventional generation, power storage systems, and power-driven cars with load needs. The article classifies EMS approaches and identifies study areas. In order to provide a continuous power supply**, [17]** suggest a DC micro grid energy management method that integrates battery energy, wind, and PV in a hybrid green power system Battery energy storage, wind turbines, and solar panels make up a hybrid clean energy system. Simulations and laboratory validation are used to assess the strategy's utilization of LSTM networks for energy generation and battery status prediction.

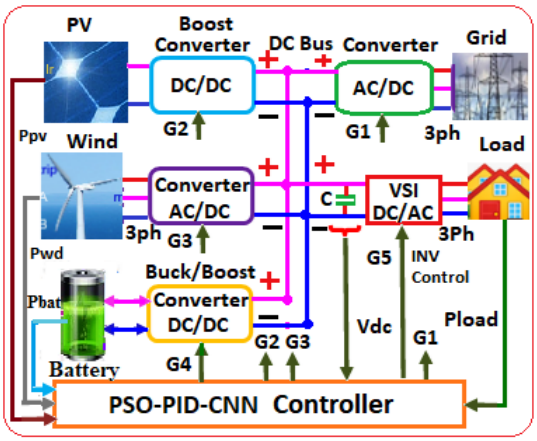

Fig. 1 System Modeling

This study's simulation model integrates a controlled grid with photovoltaic, wind, and battery energy sources, with the battery connected via a bi-directional converter and photovoltaic and wind sources via a DC/DC step-up converter system illustrated in figure 1. The existing HRESs conversion DC source is linked to a shared DC bus equipped with a capacitor. The DC power is supplied to the dynamic resistive-inductive (RL) load via a voltage source inverter that is optimally managed by the proposed EMC system.The VSI control reference signal is generated using an EMC system, comparing load parameters and DC link capacitor bus voltage. The power conversion system is managed using PSO-PI, PSO-PI-RNN, and PSO-PI-CNN controllers for energy management. The study conducted simulations to analyze the dynamic load change configurations of a (HRPS), which uses PV and wind energy, a battery for backup storage, and a controlled grid supply for responsive load management. The efficiency of the suggested methodology is illustrated using various kinds of EMS techniques and extensive simulation scenarios in the Matlab/Simulink

environment. The existing HRESs conversion DC source is linked to a shared DC bus equipped with a capacitor. The DC power is supplied to the dynamic resistive-inductive (RL) load via a voltage source inverter that is optimally managed by the proposed EMC system. Connected in parallel, the DC power conversion system delivers power to a (DC/AC) VSI inverter, which in turn is associated with a dynamic resistive-inductive load.

II. SYSTEM ARCHITECTURE

A. *System Description and Modeling*

The design of a HRPS, which integrates a controlled grid, comprises a solar photovoltaic system is connected to a direct current converter., alongside a wind turbine linked to a PMSG that interfaces with a controlled rectifier. Furthermore, the system incorporates a backup storage solution consisting of rechargeable batteries, which are managed through a bi-directional DC converter for charging and discharging. A common DC link capacitor bus serves to unify all energy sources. This common DC source is then connected to a (VSI), which supplies a dynamic AC resistive-inductive load. The entire system is governed by an energy management framework utilizing PSO-PI, PSO-PI-RNN, and PSO-PI-CNN methodologies.

B. *PV Models*

Figure 2 shows a generic model equivalent circuit with a photocurrent source, diode, parallel resistor, and series resistor. Equation (1) illustrates photovoltaic current expression in relation to solar cell circuit and Kirchhoff's circuit laws application.

$$I_{pv} = I_{ph} - I_0\left[e^{q\left(\frac{ev_d}{KFT_c}\right)} - 1\right] - \frac{V_d}{R_p} \qquad (1)$$

The equation 'Iph' represents the saturation current, 'I_{pv}' represents the photovoltaic current, 'Vd' represents the diode voltage, 'Tc' the absolute cell temperature, and 'R_p' the parallel resistance. The photocurrent 'I_{ph}' is primarily influenced by The equation (2) that follows outlines the relationship between solar insolation and the temperature of the cell.

$$I_{ph} = \left[\mu_{SC}\left(T_c - T_r\right) + I_{sc}\right]G \qquad (2)$$

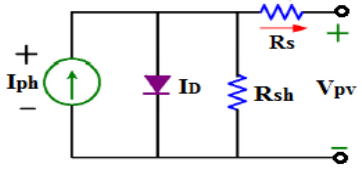

Fig. 2 PV Equivalent circuit

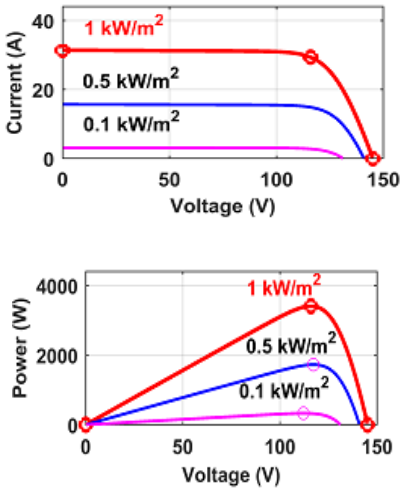

Fig. 3 P-V and I-V the characteristics

TABLE I. SPECIFICATION

Parameters	Values
Model	'Solartech ISTH-215-P'
Series conneced ,	4 Nos
Parallel Strings	4 Nos
Short circuit current(Isc)	8.95 A
Open circuit volt(Voc)	45.22 V
Module Maximum current(Imax)	8.45 A
Maximum volt (Vmax)	37.28 V
maximum Power(Pmax)	315 W

Within this framework, 'μ_{sc}' signifies the heat coefficient pertinent to the 'Isc' of photovoltaic cells. The term 'Tr' is used to denote the reference temperature of these cells, whereas 'Isc' indicates the 'Isc' at standard conditions of 25°C and 1 kW/m². Additionally, G represents the solar irradiance, expressed in kW/m² respectively. Figure 3 demonstrates the P-Vand I-V characteristics of a PV panel, produced under variable conditions of solar irradiance and temperature, represented by G(W/m²) values. The study highlights the necessity of implementing a (MPPT) algorithm to guarantee that the system consistently functions at its optimal power output

C. Wind Models

The wind system simulation model's technical parameters show table 2 that The wind facility's electrical generation is directly linked to the wind's speed. The following equations (3) through (4) can be used to express the power delivered.

$$P_t = \frac{1}{2}\rho a C_p A_t V_w^3 \qquad (3)$$

$$\lambda = \frac{\Omega_T R}{V} \qquad (4)$$

$$T_t = \frac{P_t}{\omega} = \frac{1}{2}\rho a C_p A \qquad (5)$$

TABLE II. WIND SYSTEM PARAMETERS

Parameter	Values
Wind turbine	
Velocity of wind	12m/s
Power	2.5KW
PMSG Generator details	
speed	4000rpm
DC/DC system	Diode Bridge
Voltage During Operation	100V
Current capacity	50A
Power capacity	5000 Watts

In equation (3), v_w^3 represents the wind swiftness, C_p denotes the Coefficient associated with wind energy, ρ_a indicates the air volume, "R" stands for the blade's radius., S (m²) signifies the operative surface area swept by the blade, and λ represents the pitch angle of the wind blade along with the tip speed ratio. In equation (4), 'R' and 'Ω_T' correspond to the wind turbine's rate of rotation and blade radius, respectively. The torque T' on the shaft cab be calculated using equation (5) The rotational speed (ω) is measured from PMSG's model

D. Battery energy system(BES)

The (BES) system serves as a supplementary resource for the power generator, providing crucial electricity during periods of inadequate output from RES and the grid system, employing a bi-directional (Buck-Boost) converter.

TABLE III. BATTERY PARAMETERS

Parameter	Values
capacity	50 (Ah)
Rated Voltage	370 V
Voltage Obtainable	355 (VA)
Charging ampere	21.05 (A)
Rated Charging Volt	415 (V)

$$SoC = SoC + \int_{to}^{t} \left(\frac{I_{bat}}{C_{bat}} \right) dt \qquad (6)$$

The variable I_{bat} represents the battery current, while C_{bat} denotes the battery's rating illustrate in Table 3. The recommended EMS controller regulates the available solar energy (P_{PV}) and the load power characteristic (P_L) to provide appropriate charging and discharging procedures using the buck-boost conversion system.

E. A three-phase RL loads

Dynamic variations can influence both the actual and reactive inductance loads associated with the HRPS system. The rating of the inductive load varies within a specified time interval. The system functions at a voltage level of 380 volts and a frequency of 50 hertz. In instances where renewable power is insufficient, grid power is employed to meet the power usage needs, facilitated by the proposed EMS. The specifications for the 3ph inductive load are exhaustive in Table 4.

TABLE IV. AC LOAD DETAILS

Description	Specification
Voltage	400V
Frequency	50Hz
Resistance	5KW/phase/7KW/phase
Inductance	5KVA/phase/7KVA/phase

III. POWER REGULATION CONTROL SYSTEM

Hybrid green power encompasses a diverse range of sources, which is is necessary for optimal performance of the energy management system (EMS)..The implementation of three distinct algorithms for the EMS strategy is necessary to achieve optimal performance in response to dynamic load demand fluctuations and varying configurations of hybrid renewable power systems (HRPS).

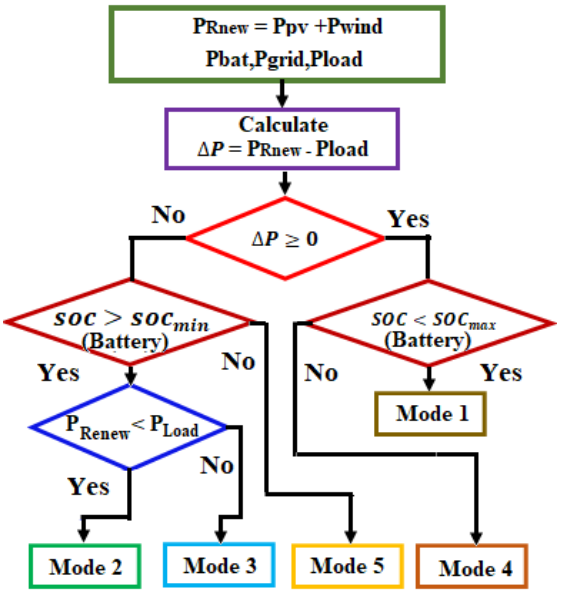

Fig.4 PMS control system based on states

The primary energy sources for photovoltaic (PV) and wind systems are characterized by their intermittent nature, which often leads to a mismatch with load demand. The discrepancy necessitates the use of additional backup systems like storage energy and the control grid to effectively manage and store renewable power. In the present work h study, the authors have designed EM control system for hybrid power systems (HPS) that integrates a PV, wind and a battery. The algorithm developed allows the adoption of different operational modes in electricity management methods, taking into account elements such as PV generator energy production, wind resources, battery levels, and SOC, as depicted in figure 4.

Mode 1: The system is designed to harness surplus power generated from PV systems, wind power, and a controlled electrical grid, thereby facilitating the management of load discrepancies through the charging of the capacitor. Mode 2: During this phase, there was a reduction in both wind speed and photovoltaic (PV) insolation, whereas the power from the grid remained constant. To produce the required power output, effective load management is crucial. Additionally, the battery was in charging mode throughout this interval.

Mode 3: In this configuration, the provision of direct current power to the load is facilitated by the grid functioning independently, accompanied by fluctuations in both photovoltaic and wind energy production.

Mode 4: The insolation from the photovoltaic (PV) system was progressively reduced, while the wind speed maintained stability as observed in the preceding mode. The battery was completely emptied, allowing the grid to effectively manage the demand, and any extra electricity was sent to recharge the battery unit.

Mode 5: The shortfall in wind energy production is offset by contributions from both the grid and the photovoltaic system.

A. Over View of PSO

A population-based technique called PSO employs particles as potential solutions to issues. These particles are governed by mathematical equations, with their movement influenced by their position and the positions of other particles. A fitness function assesses each particle's performance, identifying the optimal solution. The global optimum is determined through iterative generations within an n-dimensional search space, where particles' positions and velocities are continuously updated

$$v_i = \left[v_{i1}\ v_{i2,}\ v_{in}\right] and\ x_i = \left[x_{i1},\ x_{i2,}x_{i3}.....x_{in}\right]^{TT} \quad (7)$$

Respectively.

The position of particles signifies potential solutions within an n-dimensional search space, while their velocity reflects the variation between these positions as described in equation (8). Each particle possesses an optimal position that aligns with the best solution obtained up to the current time

$$p_i = [p_{i1}\ p_{i2}....p_{in}]^T \quad (8)$$

The global best particle, referred to as pg, signifies the most optimal particle at time t within the entire swarm, with its updated velocity determined by equation (9).

$$v_{ij}(t+1) = wv_{ij}(t) + c_1 r_1(p_{ij} - x_{ij}(t)) + x_{ij}(t) + c_2 r_2(p_{gi} - x_{ij}(t)) \quad (9)$$

$$j = 1,2,...n$$

The location of each particle is revised in every generation based on equation (10).

$$x_{ij}(t+1) = x_{ij}(t) + v_{ij}(t+1),\ j = 1,2,...n \quad (10)$$

with variables w representing inertia weight, acceleration coefficients c1 and c2 denoted by r1 and r2.

B. Design of PSO-PID Controller

This study presents a PID controller that employs (PSO) algorithms to find the optimal suited parameters for a dynamic load system. The configuration of the PID controller integrated with PSO technique is shown in the figure 5. The performance of the control scheme is significantly compromised when inappropriate values for the controller tuning constants are employed, potentially leading to instability. Therefore, it is essential to adjust the controller parameters appropriately to ensure optimal control performance through the careful selection of tuning constants.

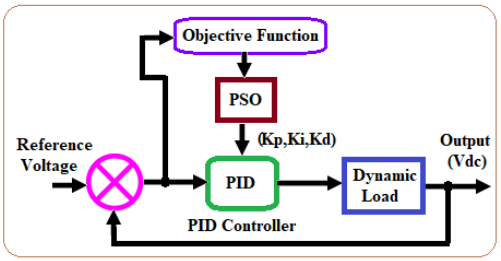

Fig.5 The block diagram illustrating the proposed PID controller integrated with PSO algorithms

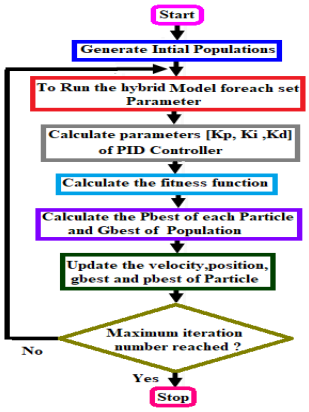

Fig. 6 PSO-PI configuration

In contrast to traditional methods that eliminate particles with unfavorable costs while reproducing those with favorable costs, the integration of particle clusters enables the utilization of identical positions within the optimal solution space. The 'i^{th} 'element, which is different from the optimal particle, is situated at multiple points on the surface of a virtual sphere that is centered on the location of the 'i^{th}' particle, with the radius defined as the Euclidean distance between this particle and the best one. The best particle should be updated by comparing the costs of new positions with the cost of the previously identified best particle.

The optimal particle diffuses attractant to other particles within a cluster, forming 'cones of attraction' with axes connecting them to the remaining particles. The process depends on maintaining an angle between the optimal particle and the current and subsequent positions of the i^{th} particle within specified degrees. The Particle Swarm Optimization (PSO) approach uses three-dimensional components (P, I and D) for particles, requiring them to navigate within a three-dimensional environment. Figure 6 illustrates the PSO-PID control system. Selection parameter of PSO and optimized PI parameters described in table 5 and six respectively. The primary objective function utilized for the optimization of PID parameters is the ITAE performance index, with the goal of minimizing the performance index of the feedback control system The PI parameters are obtained for 15 iterations.

$$ITAE = \int_0^{\infty} t \left| e^t \right| \partial t \qquad (10)$$

TABLE V. SELECTION PARAMETER OF PSO

Population size	5
Iteration count	15
Constant of Velocity (c1)	01.19
Contant of Velocity (c2)	01.49

TABLE VI. TABLE 6 OPTIMIZED PI PARAMETERS

Tuning Method	Kp	Ki	Kp
Ploe placement	11.78	3.13	16.23
PI-PSO (ITAE)	4.16	5.16	6.17

The PSO algorithm is an M file that interfaces with a Simulink model. It transmits initial particle values to the Simulink module, which calculates fitness values based on ITAE standards of performance. The process continues iteratively until satisfactory performance criteria are reached. The optimal control parameters for both classical and proposed PID controllers are presented.

C. Recurrent Neural Network

RNNs were developed specifically for the analysis of time-series data and have demonstrated effectiveness across numerous fields, such as speech recognition, machine translation, and image captioning. RNNs handle incoming time-series data by processing individual vectors sequentially, while maintaining the information from prior time steps in a hidden state.

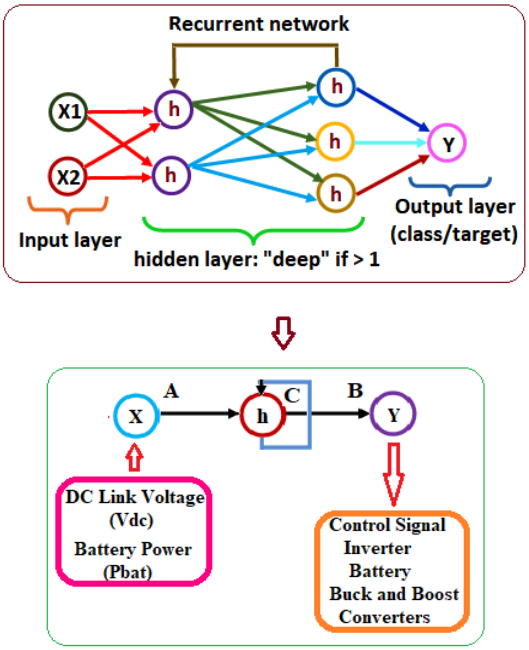

Fig.7 RNN (a) Structure (b) Flow Control

$$h(t) = f_c \quad (h(t-1)), x(t) \qquad (11)$$

Here, h(t) signifies the present state, 'fc' is a role assigned the value 'c', h(t-1) corresponds to the prior state, and x(t) is the input matrix at the time step 't'. Figure 7 depicts the configuration of the system. where "x" denotes the input layer. This layer is responsible for gathering real-time data from the hybrid renewable system, encompassing 1250 control parameters that pertain to critical environmental conditions. Among these parameters, Power net (Pnet) of PV, wind, DC link voltage(V_{dc}), load power and battery power are particularly influential on crop productivity. The hidden layer is represented by "h," while "y" signifies the output layer. The resulting output is achieved by employing the optimal modulation index for bi-directional battery converters in conjunction with the RL load inverter, with the current input comprising values from x(t) and x(t-1) at certain moments, hence enhancing the network's efficiency

D. CNN algorithm

The CNN are an advanced type of ANN that are particularly adept at processing time-series data. A CNN is fundamentally organized into three key players: the convolution layer, the pooling layer, and the fully connected layer, which is denoted in Figure 8. with the training process illustrated in Figure 9. The input layer gathers real-time data from agricultural settings, integrating 1,200 control parameters that influence Power net (P_{net} = PV+Wind), DC link voltage (V_{dc}), load power and battery power content. The convolutional layer primarily serves to identify local features within the input data, while the pooling layer plays a major role in decreasing the dimensionality of this data. By minimizing the dimensions of feature representations, the pooling layer alleviates memory and computational demands as the depth of the network escalates. In contrast, fully connected layers are essential for generating high-level representations and facilitating the prediction of the system's control parameters.

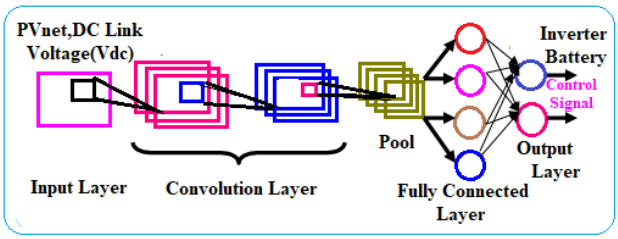

(a)

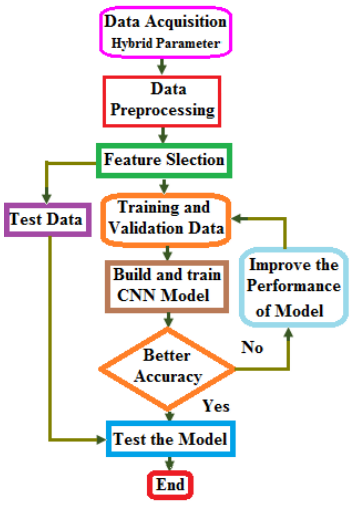

(b)

Fig. 9 CNN(a) Architecture (b)Functional flow chart

The essential concept of convolution forms the basis of a CNN. In the CNN we introduce, there are two key components: the convolution layers, as outlined in Equations (5) and (7), and the pooling layer. The core role of the pooling layer is to minimize the amount of constraints in the tensor by decreasing its dimensions, thus facilitating a decrease in computational time.

$$y_j^{(1)} = (t_i^{i-1}) \times w_{ij}^i + b_j^t \quad (5)$$

$$t_j^i = f\left(y_i^i\right) \quad (6)$$

$$f(x) = \max(0, x) \quad (7)$$

The convolution layer interrelates with the convolutional kernel to produce output feature graph j, which may result from multiple input feature graphs. It is defined by c_j, b_j^l, y_j^l,and $w_{ij}^{(l)}$ the convolution kernel (8).t_j^l Equation (9) depicts the feature graph related to the convolution layer l.The symbol for the activation function is '*f*'. As stated in Equation (9), will adopt a rectified linear unit (ReLU) in this study equation (9).The algorithm develops an optimal CNN controller using real-time data from the agricultural sector, enhancing charging and discharging efficiency by identifying globally optimal parameters for bi-directional battery converters and pump controllers through CNN algorithms.

IV. SIMULATION AND RESULTS

The essential RES are wind and PV energy, battery and supportive components of a controlled grid are utilized to manage dynamic loads. To evaluate the precision of the control algorithms, a model using Simulink has been designed. of PSO-PID, PSO-PID-RNN, and PSO-PID-CNN controllers, aimed at regulating the DC bus voltage and facilitating DC/AC conversion inverters under conditions of varying resistive-inductive (RL) loads. The simulation model is illustrated in Figure 10 and was executed using the MATLAB/Simulink platform, incorporating various configurations of the available natural resource parameters.

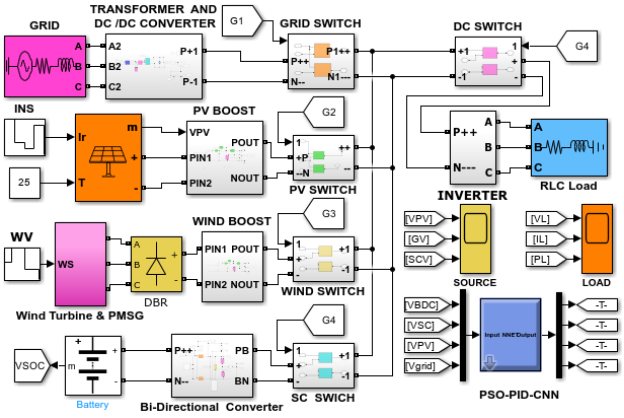

Fig. 10 Simulation Model

The EMC controller is responsible for generating three control signals: S_{pv}, S_{wind}, S_{grid}, and S_{bat}, based on three input variables for battery storage unit performance include irradiation (G), wind speed, and battery (SOC).. Figure 4 illustrates the operational flow chart. The system can operate in five distinct modes, with energy delivered to the load as illustrated by balance equation (20).

$$P_{load}(t) \pm S_{BAT} = P_{pv}(t) \times S_{pv} + P_{wind}(t) \times S_{wind} + P_{grid}(t) \times S_{grid} \quad (10)$$

The battery is charged when the hybrid power surpasses the load, and discharged when the load is less than the hybrid power.

Where: S_{pv}: Control signal of the PV, S_{wind}: Wind Control signal S_{grid}: Grid Control signal and S_{bat}: Control signal of Battery.

The simulation carried out the configuration

- Dynamic load conditions

To evaluate how well the implemented simulation of the RES system works. A simulation of five configurations over 0 to 0.9 seconds showed various source components, including PV insolation, wind velocity, and battery energy system state of charge.

Mode of operation

Mode l: (0.0s <t<0.15s): The PV, wind source, and grid are interconnected for (0.0 s to 0.15s), with PV irradiation measured at 500 W/m² and wind velocity 9 m/s. At this stage, the storage battery triggers the start of the charging process.

Mode 2: (0.15s <t<0.3s): A wind velocity of 5 m/s is associated with a PV irradiation of 250 W/m² in conjunction with the grid. The battery is continuously kept in charging mode with this setup.

Mode 3 3(0.3s <t<0.6s): this configuration, the grid voltage is isolated while exists a correlation between wind velocity and photovoltaic insolation, with respective values of 9 m/s and 1000 W/m. he battery starts to release its charge to the connected load

Mode 4 (0.6s <t<0.75s): The photovoltaic insolation is measured at 750 W/m², accompanied by a wind speed of 3 m/s. The system operates in grid-isolated mode, with a battery configured for charging.

Mode 5 (0.75s <t<0.9s): In this sequence, the grid has been restored. with a photovoltaic (PV) insolation of 750 W/m² at a voltage of 750 V_{dc}, accompanied by a wind speed of 3 m/s, while the system operates in battery charging mode.

TABLE VII. HYBRID SOURCES

Configuration	Simulation duration(s)	Wind elocity(m/s)	PVInsolation (W/m²)	battery Voltage(V_{dc})		Grid Voltage(V_{dc})
				Charge	Discharge	
TR1	0-.15	9	500	-21.62	-	750
TR2	0.15s-0.3s	5	250	-21.62	-	750
TR3	0.3s-0.45s	9	1000	-	20.87	0
TR4	0.45s-0.6s	9	1000	-	20.81	0
TR5	0.6s-0.75s	3	750	-21.62	-	750
TR6	0.75s-0.9s	3	000	-21.62	-	750

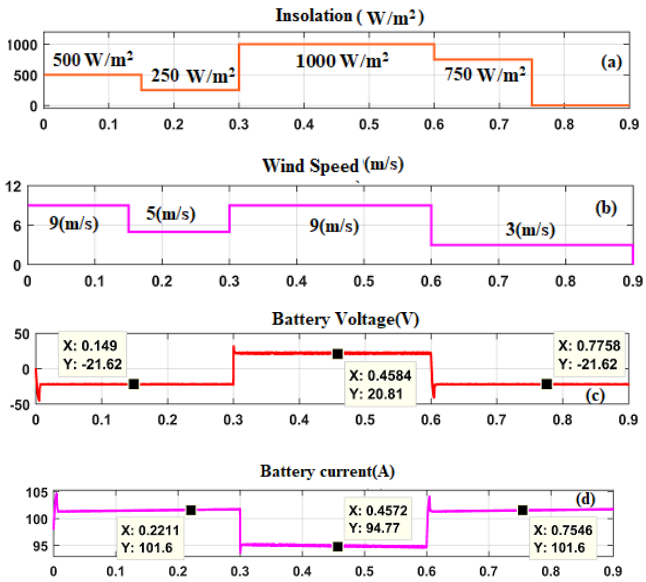

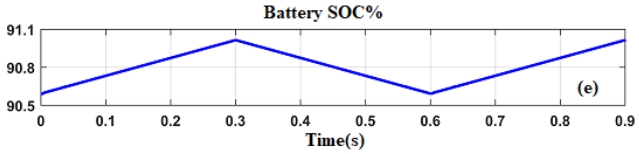

Fig. 11 RES parameter (a) PV Insolation, (b) Turbine speed, (c) battery voltage (d) Battery Current(e) Battery-SOC

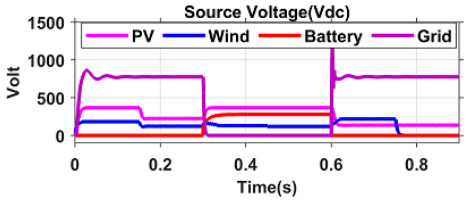

Fig. 12 Source Voltages (V)

The voltage produced by a hybrid renewable source's direct current conversion prior to the inclusion of an EMC controller is seen in Figure 12. Figures 13 (a) to (c) demonstrate the EMC control signal configurations, specifically the Modulation Index, along with a detailed view of each configuration. In Figures 14 (a), (b), and (c), Presented herein are the RMS values of voltage, current, and power for the three-phase RL load.

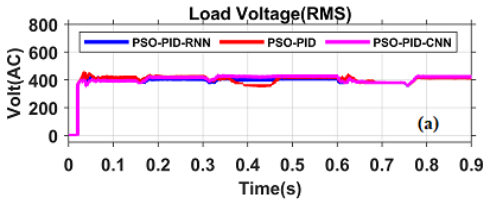

A. Dynamics Load

The RL circuit dynamically altered the values of a specified interval under varying operational climatic conditions of renewable hybrid system of PV, Wind and fluctuating grid voltage, while monitoring the transient behaviors of voltage, current, and power. The framework for the control signal generated by the proposed EMC system is defined by the accessible RES and their corresponding load demands.

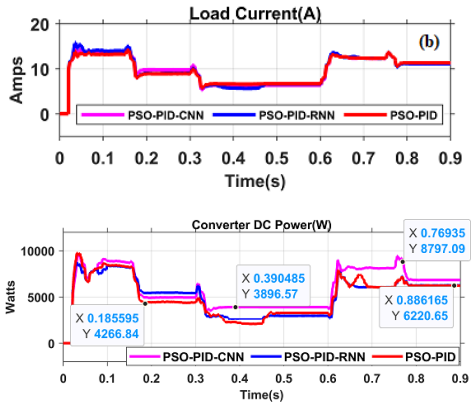

Fig. 13 Converter DC (a) voltage (b) Current (c) Power

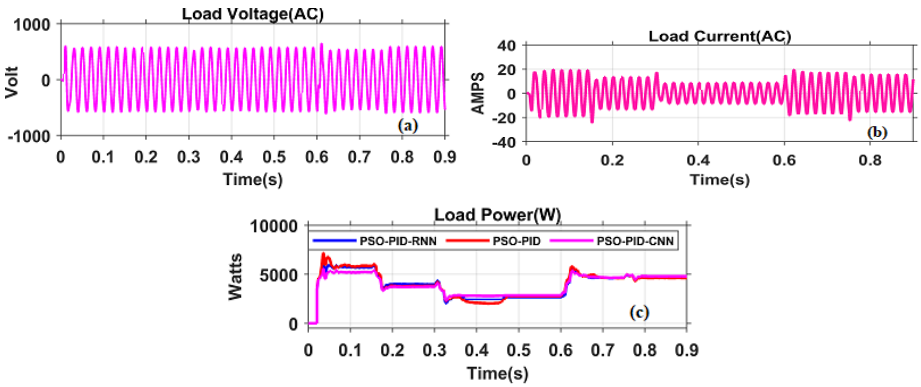

Fig. 14 Dynamic Load (a) Load Voltage (b) Load current (c)RMS Power

Figure 14 (a) to (c) illustrates the AC voltage, current and RMS value of power to the allocation of the load to three individual controllers. In the frame work utilizing the PSO-PID control strategy is applied, the transient voltage overshoot reaches 431.20V in response to fluctuating load conditions, while the input source voltage experiences an undershoot of 348.00V. In contrast, the PSO-PID-RNN configuration results in voltages of 440.40V and 361.40V, whereas the PSO-PID-CNN configuration yields values of 334.00V, and 420.90V respectively. The numerical results of the RMS load voltage for all six configurations are presented in Table 8. The analysis presented in Figure 12(b) reveals the simulated outcomes of dynamic load current, which are further detailed in Table 9. The conventional PSO-PID controller exhibits TR 1 (0s-0.15s) configuration a transient current oscillation of 14.70 A, with an undershoot of 6.01 A and settling at 13.50A. In contrast, the intelligent algorithms, namely PSO-PID-RNN and PSO-PID-CNN, demonstrate transient currents of 14.97 A and 8.31 A, as well as 13.52 A and 8.35 A, respectively.

TABLE VIII. LOAD VOLTAGE

Simulation configuration	**PSO-PID**		**PSO-PID-RNN**		**PSO-PID-CNN**	
	Transient	Steady state	Transient	Steady state	Transient	Steady state
TR1	141.40	405.15	440.40	403.40	344.00	381.00
TR2	382.60	400.70	380.80	405.50	360.40	400.70
TR3	345.90	399.40	361.40	406.50	368.50	410.90
TR4	365.80	400.50	379.10	406.00	367.70	397.60
TR5	375.40	412.30	372.90	401.70	370.40	408.50
TR6	420.88	416.27	422.061	418.64	426..292	421.561

TABLE IX. LOAD CURRENT

Simulation configuration	PSO-PID		PSO-PID-RNN		PSO-PID-CNN	
	Transient	Steady state	Transient	Steady state	Transient	Steady state
TR1	13.83	13.50	14.97	13.38	12.99	12.47
TR2	8.373	8.306	14.39	8.31	13.52	8.35
TR3	9.46	5.783	9.45	6.03	9.41	6.12
TR4	12.79	12.68	12.85	12.98	12.74	12.84
TR5	14.10	10.70	14.22	10.55	14.08	10.80
TR6	13.62	11.33	13.62	11.12	13.56	11.24

TABLE X. CONVERTER DC POWER

Simulation configuration	PSO-PID		PSO-PID-RNN		PSO-PID-CNN	
	Transient	Steady state	Transient	Steady state	Transient	Steady state
TR1	9488	8898	6185	5822	5620	5249
TR2	7133	4921	3368	3811	3461	3829
TR3	6303	3536	1942	2736	2204	3004
TR4	9429	8113	5676	5599	5639	5662
TR5.	8156	6828	4510	4825	4582	4901
TR6	7194	6219	7216	6255	7153	6828

TABLE XI. AC LOAD POWER

Simulation configuration	PSO-PID		PSO-PID-RNN		PSO-PID-CNN	
	Transient	Steady state	Transient	Steady state	Transient	Steady state
TR1	7201	5914	6185	5822	5620	5249
TR2	3475	3784	3368	3811	3461	3829
TR3	2188	2927	1942	2736	2204	3004
TR4	5683	5780	5676	5599	5639	5662
TR5	4476	4745	4510	4825	4582	4901
TR6	4676	4619	4735	4702	4939	4778

Figure 12(c) and Table 10 provide a comparative analysis of all configurations (TR1-TR6) the simulated and numerical results concerning the of dynamic RL loads. During the interval from 0 s to 0.15 s, when a load of RL (7.5 KW + 7.5 KVAR) is connected, the observe simulated output converter dc transient power 9488W and settling steady state at 8988W in the algorithm of PSO-PID, as well as the PSO-PID –RNN and PSO-PID CNN, transients and settling power of 6185W and 5822W and 5620Wand 5249W respectively, all six configuration of converter simulated response presented in table 10. In the configuration of ac RMS power transient power recorded is 7201 W, stabilizing at 5914 W under the PSO-PID controller. Conversely, the PSO-PID-RNN controller achieves a power output of 6185 W, an increase from the stable output of 5822 W, the PSO-PID-CNN ultimately achieves an overshoot of 5620W and stabilizes at 52249W, respectively. All the six load configuration of ac RMS power details display the table 11. The examination of both static and dynamic outcomes reveals that the PSO-PID-CNN power management system effectively reduces both The enhancement of settling time within the simulation environment, along with the management of upper and lower peak transients and oscillations.

V. CONCLUSION

This study has examined the comparative output responses of four distinct modeled EMC controllers for the controlled grid-integrated HRPS. The HRPS was developed and verified using simulations conducted in MATLAB. The simulations were evaluated under both constant and fluctuating conditions, considering different durations and environmental factors affecting renewable resource generation. The overall results detailing the transient and The settling periods for current, voltage, and power to the load are included in the data that is demonstrated. Through both simulation and numerical validation. Observational results indicate that the PSO-PID-CNN controller demonstrates a significantly response compared to the other three control strategies.

REFERENCES

[1] Basaran, K., Cetin, N. S., &Borekci, S. (2017). “Energy management for on-grid and off-grid wind/PV and battery hybrid systems”. IET Renewable Power Generation, *11*(5), 642-649

[2] Ge, X., Ahmed, F. W., Rezvani, A., Aljojo, N., Samad, S., &Foong, L. K. (2020). Implementation of a novel hybrid BAT-Fuzzy controller based MPPT for grid-connected PV-battery system.*Control Engineering Practice*,*98*, 104380.

[3] Benlahbib, B., Bouarroudj, N., Mekhilef, S., Abdeldjalil, D., Abdelkrim, T., &Bouchafaa, F. (2020). Experimental investigation of power management and control of a PV/wind/fuel cell/battery hybrid energy system microgrid. *International Journal of Hydrogen Energy*, *45*(53), 29110-29122.

[4] Nasef, S., Hassan, A., ElMadany, H., Zahran, M., EL-Shaer, M., &Abdelaziz, A. (2022). Optimal power management and control of hybrid photovoltaic-battery for grid-connected doubly-fed induction generator based wind energy conversion system. *International Journal of Renewable Energy Research*, *12*(1), 408-421.

[5] El-Sattar, H. A., Kamel, S., Sultan, H., Tostado-Véliz, M., Eltamaly, A. M., &Jurado, F. (2021). Performance analysis of a stand-alone pv/wt/biomass/bat system in alrashda village in egypt. *Applied Sciences*, *11*(21), 10191.

[6] AbouHouran, M., Bukhari, S. M. S., Zafar, M. H., Mansoor, M., & Chen, W. (2023). COA-CNN-LSTM: Coati optimization algorithm-based hybrid deep learning model for PV/wind power forecasting in smart grid applications.*Applied Energy*,*349*, 121638.

[7] Assem, H., Azib, T., Bouchafaa, F., Laarouci, C., Belhaouas, N., &Hadj Arab, A. (2023). Adaptive Fuzzy Logic-Based Control and Management of Photovoltaic Systems with Battery Storage. *International Transactions on Electrical Energy Systems*, *2023*(1), 9065061.

[8] Priya, S., Sridevi, V., Batumalay, M., &Gunapriya, D. (2024). Convolutional Neural Network for Battery System Monitoring and SOC Estimation for Ev Applications to Achieve Sustainability. *Journal of Applied Data Sciences*, *5*(4), 1802-1813.

[9] Almashnowi, M. Y., AlGhamdi, S., Alamier, W. M., Ali, S. K., Bakather, O. Y., Hassan, M., &Alam, M. M. (2024). A Hybrid Deep Learning-Based Power Management Strategy for PV-Assisted Desalination Plant. *Particle & Particle Systems Characterization*, 2400053.

[10] Shekhar, H., BhushanMahato, C., Suman, S. K., Singh, S., Bhagyalakshmi, L., Prasad Sharma, M., ... &Rajaram, A. (2023). Demand side control for energy saving in renewable energy resources using deep learning optimization. *Electric Power Components and Systems*, *51*(19), 2397-2413.

[11] Aslam, S., Kumar, K. V., Babu, T. A., & Rajesh, P. (2025). Hamiltonian deep neural network technique optimized with lyrebird optimization algorithm for detecting and classifying power quality disturbances in PV combined DC microgrids system. *Environment, Development and Sustainability*, 1-24.

[12] Rehman, A. U., Hafeez, G., Albogamy, F. R., Wadud, Z., Ali, F., Khan, I., & Khan, S. (2021). An efficient energy management in smart grid considering demand response program and renewable energy sources. *IEEE Access*, *9*, 148821-148844.

[13] Vijayakumar, B., Purushothamarn, K. E., Khabiya, P., Garg, A., Rajesha, N., &Kaliappan, S. (2024, October). Improving Microgrid Reliability and Efficiency Through Energy Storage Systems with a Pyramidal Dilation Attention Convolutional Neural Network for Renewable Energy Integration. In *2024 4th International Conference on Sustainable Expert Systems (ICSES)* (pp. 1756-1762). IEEE.

[14] Naceur, F. B., Salah, C. B., Telmoudi, A. J., &Mahjoub, M. A. (2021). Intelligent approach for optimal sizing in photovoltaic panel-battery system and optimizing smart grid energy. *Transactions of the Institute of Measurement and Control*, 01423312211027027.

[15] Tajjour, S., &Chandel, S. S. (2023). A comprehensive review on sustainable energy management systems for optimal operation of future-generation of solar microgrids. *Sustainable Energy Technologies and Assessments*, *58*, 103377.

[16] Vuddanti, S., &Salkuti, S. R. (2021). Review of energy management system approaches in microgrids. *Energies*, *14*(17), 5459.

[17] Mahjoub, S., Chrifi-Alaoui, L., Drid, S., &Derbel, N. (2023). Control and implementation of an energy management strategy for a PV–wind–battery microgrid based on an intelligent prediction algorithm of energy production. *Energies*, *16*(4), 1883.

[18] Ramesh, T., Balachander, K., (2024).Optimizing hybrid renewable energy systems with integrated electric vehicle using a hybrid approach, Science Direct, Journal of Energy Storage Volume 89,111655.

Ramesh T received the Diploma with first class honors from the Nachimuthu Polytechnic, TamilNadu, India, in 2001, B.Eng. and M.Eng. degrees from the Government College of Technology, TamilNadu, India, in 2007 and 2009, respectively and is currently pursuing the Ph.D. degree at Karpagam Academy of Higher Education, TamilNadu, India. From 2009 to 2018, he was an Assistant Professor with the Karpagam Academy of Higher Education, TamilNadu, India and from 2019 to 2021, he was a tenured as Research Instructor in TRIOX Technology. From 2022 onwards, he is a tenured Associate Professor with the Park College of Engineering and Technology, TamilNadu, India. He is also a member of ISTE, IE (I), IAEMP, ISRD. His areas of interests are Renewable Energy, Smart grid and Internet of Things (IoT).

Balachander Kalappan received the Diploma in Electrical and Electronics Engineering from PSG Polytechnic, Coimbatore in 1993 and Bachelor degree in Electrical and Electronics Engineering from Coimbatore Institute of Technology, Coimbatore in 2001. He acquired Master of Engineering in VLSI Design from Anna University Coimbatore in 2009, PG Diploma in Electrical Energy Management and Auditing from Annamalai University, Chidambaram in 2015 and Doctorate in Electrical and Electronics Engineering from Karpagam Academy of Higher Education, Karpagam University, Coimbatore in 2017. He is working as an Associate Professor in Department of Electrical and Electronics Engineering, Faculty of Engineering, Karpagam Academy of Higher Education, India. He has totally around 15 years of teaching experience and 7 years of industry experience. He has published around 90 National and international Journal papers and 25 papers in Conference proceedings. He is a recognized reviewer in many reputed journals like Springer, Inderscience, etc. He is also a member of ISTE, IE (I), IAENG, IRED, IACSIT. His areas of interests are Renewable Energy, Smart grid and Distributed Generation.